3.4. CRÈME96 and Related Error Rate Prediction Methods

James H. Adams, Jr., NASA Marshall Space Flight Center

1. Introduction

Predicting the rate of occurrence of single event effects (SEEs) in space requires knowledge of the radiation environment and the response of electronic devices to that environment. Several analytical models have been developed over the past 36 years to predict SEE rates. The first error rate calculations were performed by Binder, Smith and Holman [1]. Bradford [2], [3] and Pickel and Blandford, in their CRIER (Cosmic-Ray-Induced-Error-Rate) analysis code [4], [5], introduced the basic Rectangular ParallelePiped (RPP) method for error rate calculations. For the radiation environment at the part, both [3], [2] and [5] made use of the Cosmic Ray LET (Linear Energy Transfer) spectra calculated by Heinrich for various absorber depths [6]. A more detailed model for the space radiation environment within spacecraft was developed by Adams and co-workers [7]-[14]. This model, together with a reformulation of the RPP method published by Pickel and Blandford [5], was used to create the CRÈME (Cosmic Ray Effects on Micro-Electronics) code [15], [16]. About the same time Shapiro wrote the CRUP (Cosmic Ray Upset Program) [17] based on the RPP method published by Bradford [2]. It was the first code to specifically take into account charge collection from outside the depletion region due to deformation of the electric field caused by the incident cosmic ray. Other early rate prediction methods and codes include the Single Event Figure of Merit [18], NOVICE [19], the Space Radiation code [20] and the effective flux method of Binder [21] which is the basis of the SEFA (Scott Effective Flux Approximation) model [22].

By the early 1990s it was becoming clear that CRÈME and the other early models needed

revision [23], [24]. This revision, CRÈME96 [25], was completed and released as a WWW-based tool, one of the first of its kind. The revisions in CRÈME96 included improved environmental models and improved models for calculating single event effects. The need for a revision of CRÈME also stimulated the development of the CHIME (CRRES/SPACERAD Heavy Ion Model of the Environment) [26] and MACREE (Modeling and Analysis of Cosmic Ray Effects in Electronics) [27]. The Single Event Figure of Merit method was also revised to use the solar minimum galactic cosmic ray spectrum [28] and extended to circular orbits down to 200 km at any inclination [29]. More recently a series of commercial codes was developed by TRAD (Test & Radiations) which includes the OMERE code [30] which calculates single event effects.

There are other error rate prediction methods which use Monte Carlo techniques. These will be discussed in chapter 3.5 “MRED and Monte Carlo Based Tools”. In this chapter the analytic methods for estimating the environment within spacecraft will be discussed.

2. The Radiation Environment

The principle components of the interplanetary space radiation environment are galactic cosmic rays (GCRs), solar energetic particles (SEPs), and trapped radiation. In addition to these, there are some minor components that usually do not play an important role in causing single event effects. These are the anomalous cosmic rays and particles accelerated in co-rotating interaction regions. While the anomalous component is a minor contributor in the neighborhood of the Earth it makes an important contribution to the ionizing radiation environment in the outer heliosphere.

For satellites in Earth orbit, the interplanetary environment must be modulated by the

orbit-averaged effect of the Earth's magnetic field. Satellites also encounter the radiation trapped in the Earth's magnetic field. In all cases, the radiation environment as the surface of the spacecraft will be modified by passage through spacecraft material on its way to the electronic components within. These aspects of error rate prediction were recently reviewed by Janet Barth [31].

2.1 Galactic Cosmic Rays

GCRs include all the nuclei of all the elements in nature. Their abundances are roughly the same as the general abundance of elements in the solar system [32]. Except for the heaviest elements, all the nuclei are completely stripped of their orbital electrons during their passage through the interstellar medium. GCRs originate from sources far away in our Galaxy. The origin of GCRs has not yet been determined; however, there is circumstantial evidence, based on the power budget for sustaining the GCR flux in the galaxy [33] that GCRs are accelerated by supernovae. Eighty to ninety percent of the core-collapse supernovae occur in OB associations (associations of O and B type stars) [34] and there is experimental evidence from the composition of GCRs that they come mostly from these OB associations [35]. During their propagation through the Galaxy between their sources and the solar system, GCRs traverse 6 to 10 g/cm^2 of interstellar matter [36]. This alters their composition, enriching GCRs in certain elements, notably Li, Be and B and the elements just below Fe.

The GCR flux outside the heliosphere is isotropic except at very high energies. To reach Earth, the GCRs must penetrate the heliosphere, overcoming the influence of the outward flowing solar wind [37]. The GCRs must diffuse upstream in the solar wind, while losing energy due to the diminishing magnetic field strength in the adiabatically expanding solar wind. This

alters the power-law GCR spectrum outside the heliosphere to the familiar form measured at Earth and shown as the dashed and chain-dash curves in figure 1, but the flux reaching 1 AU (Astronomical Unit) remains isotropic.

(Insert figure 1 here)

The model for the GCR spectrum used in CRÈME86 [8] was the result of fitting the data available by the early 1980's. At that time the GCRs were known to be modulated with the period solar activity cycle, but the difference in modulation during the even- and odd-numbered cycles had not yet been discovered, so the variation of GCR modulation with time was modeled as a sinusoidal function the same period as the sunspot cycle. Later, in 1992, Nymmik developed an improved model for the GCR spectra at Earth [38] which was adopted as the ISO standard. This model was used in the revision of CRÈME to create CRÈME96.

2.2 Solar Energetic Particles

As their name suggests, SEPs are accelerated at the Sun. They are accelerated in Solar Particle Events (SPEs) resulting from explosive releases of energy stored in the magnetic fields near the surface of the Sun. SPEs seemingly occur at random, but careful examinations of the non-potential energy stored in the sun can show when the "stage is being set" for a SPE [39]. Also SPEs are sometimes triggered sympathetically by preceding events as occurred in the 2003 Halloween event series [40] is an example. The frequency of events varies with the solar activity cycle, peaking during the active phase of the cycle.

Like GCRS, SEPs are believed to consist of all the nuclei of all the elements in nature. While their composition is also similar to the general abundance of elements in the solar system,

variability is seen from event to event. The reasons for this variability are thought to be related to their acceleration process [41] and the seed population from which they are selected for acceleration [42]. Except for the lightest particles, SEP nuclei may not be completely stripped of their orbital electrons. The variability of the ionic charge state of SEPs seems to be related to the temperature of the seed population [43], [44] and the acceleration process [45].

There are two acceleration processes for SPEs [41] resulting in impulsive and gradual events. As the name implies, the impulsive events are short-lived and are far more numerous and typically much smaller than gradual events. Large impulsive events are rare. Impulsive events are described in [45] and references therein. The acceleration sites of impulsive events are thought to be localized on the Sun near the sites of solar flares, but this remains to be proved. They are highly enriched in ^{3}He and also enriched in heavier elements, having a Fe/O ratio of ~10.

Gradual events are accelerated by shocks driven by coronal mass ejections (CMEs) [46]. Acceleration begins more than a solar radius above the surface of the Sun where the CME becomes supersonic and continues along the shock front as it expands outward into interplanetary space. This acceleration sometimes continues until the shock reaches Earth. The material accelerated in gradual events comes from suprathermal tail of the solar wind in the corona. There sometimes may be a contribution from particles accelerated to suprathermal energies by preceding impulsive events [42], but the composition does not show the strong deviations from the general abundance of elements that is seen in impulsive events.

At the time CRÈME86 was written, all SEPs were thought to be accelerated by solar flares. For this reason, all available data were used to derive the elemental composition of SEPs.

Because the instruments of the time mostly measured low energy SEPs, the data were mostly from impulsive events. This resulted in a significant over-estimate of the heavy ion content in large SPEs which are usually gradual. The ionic charge state of SEPs was also unknown at the time CRÈME86 was written, so SEPs were assumed to be bare atomic nuclei like galactic cosmic rays.

(Insert figure 2 here)

The trajectories of SPEs from their acceleration site outward into the heliosphere are guided by the interplanetary magnetic fields. Figure 2 shows the gyroradii of solar energetic protons at 1 AU as a function of their pitch angle for three different energies. Solar heavy ions have gyroradii that are 2 to 4 times larger depending on their charge state, but in all cases the gyroradii of SPEs are small compared to 1 AU. As a result, SPEs accelerated near the sun closely follow their guiding center field line out into the heliosphere. When the interplanetary field is undisturbed, the rotation of the sun causes it to form a Parker Spiral [47] as depicted in figure 3. In this case, the guiding center field line spirals out from the Sun smoothly with the field strength diminishing as the square of the distance. The diminishing field strength adiabatically focuses [48] the flow of SEPs. Regardless of their initial pitch angle, by the time SEPs reaches 1 AU, their pitch angle has rotated to nearly align their velocity vector with the guiding field direction so the first SPEs to reach 1 AU are streaming along the field. This also has the effect of reducing their gyroradius as shown in figure 2. If the acceleration site at the sun is magnetically well connected to the Earth, The first particles to arrive will come at ~45° to the Sun-Earth line and approximately in the ecliptic plane.

(Insert figure 3 here)

Of course, a perfect Parker Spiral field configuration is never realized. There are always some magnetic field irregularities causing deviations from the Parker Spiral. These deviations will cause pitch angle scattering if the scale of the irregularity is comparable to or smaller than the distance a particle moves along the field line in a single gyroration. The effect of many such irregularities is to cause the particles to diffuse along the guiding field rather than simply streaming. This will delay the arrival of the fastest particles at 1 AU and result in the first particles having a mixture of energies. Even if there are few scattering centers between the Sun and 1 AU, the particles continue along the field beyond 1 AU and eventually encounter irregularities that scatter them, including reversing their pitch angle so that they spiral back toward Earth. For particles streaming back toward the sun, adiabatic defocusing occurs so that their pitch angles increase, eventually reaching 90° which cause them to mirror and stream away from the Sun once again. In this way the same particle usually passes 1 AU several times. The net result is that the flux arriving at 1 AU soon becomes isotropic even if it began as a unidirectional flow coming from the local interplanetary magnetic field direction.

Another consequence of pitch angle scattering is that the SPE flux at Earth often takes several days to decay, with particles continuing to arrive long after SPE acceleration has apparently ceased. This gives particles time to diffuse (or drift if a local gradient in the field is present) onto new field lines so that the SPE spreads in heliographic longitude. The result is that SPEs, not initially magnetically connected to Earth, will eventually be observed at Earth. This longitudinal spread of SPEs is not well understood. In the case of gradual events, it is at least partly due to the extended acceleration site along the expanding shock front, but propagation effects in the interplanetary medium (as discussed above) can also be partially responsible. To investigate this Wiedenbeck and co-workers [49] have examined several impulsive events using

simultaneous ^{3}He measurements from the two STEREO spacecraft and the ACE spacecraft located near Earth. They report typical longitudinal spreads of >60° with one event having a 136° spread.

The models for SPEs used by analytic error rate prediction methods consist of identifying worst-case events at various estimated levels of confidence. In CRÈME86, four reference SPE cases were presented to cover the variability in both flux and composition:

1) 10%[1] worst-case flux with mean elemental composition

2) 10% worst-case flux with worst-case composition

3) Composite worst-case flux with mean elemental composition

4) Composite worst-case flux with worst-case composition

As mentioned above, the SEP composition model in CRÈME86 overestimates the heavy ion content of SPEs. This is especially true of models 2) and 4) that include the worst-case composition. The composite worst-case flux came from combining the worst features of the Feb. 23, 1956 event and the August 4, 1972 event [50].

The CRUP program used the LET spectra from Adams [7]. The Single Event Figure of Merit [18] used the 10% worst case given by Adams [7] and shown as the chain-dot curve in figure 1. The 10% worst case is a composite environment including the galactic cosmic ray spectrum, SPEs and contributions from anomalous cosmic rays and co-rotating interaction regions. The space radiation environment should be more severe only 10% of the time.

---

[1] Only 10% of the SPEs will be more severe

The NOVICE model offers the CRÈME86 SPE models and a version of the JPL Model [51] where the Monte Carlo approach has been replaced with a numerical integration method. The CHIME model [26] offers models for SPEs based on the events measured during the CRRES satellite mission [52]. These include models for the events of March and June, 1991. In addition CHIME implements the JPL Model, a probabilistic model for SPE occurrence that gives the worst-case proton fluence as a function of confidence level.

The MACREE model [27] is a re-write of CRÈME86, to make some improvements. The principle improvement is in the SPE models. MACREE uses the October 1989 event as a model worst-case event, pointing out that it is at the 99% confidence level for proton fluencies above 10, 30 and 60 MeV according to the JPL Model. MACREE also uses improved elemental abundance for SPE heavy ions, including trans-iron ions. In addition, it takes into account an estimate of the mean ionic charge state of SPE heavy ions.

Space Radiation [20] offers several SPE models to choose from. The SOLPRO model [53] is offered. Also included are a collection of flux and fluence models for both individual extremely large events and composite events. Among these are the CRÈME86 SPE models [8], additional heavy ion models based on CRÈME86 that are said to be somewhat improved, the King model [54], a model for the total fluence of the October 1989 event [55] and several models developed at Aerospace Corp. [56] in response to the shortcomings of the CRÈME86 models. These include models for the proton peak flux and event-integrated fluence for the events of August, 1972 and October, 1989. The authors also provide a worst-case composite of these two events. Space Radiation also includes the improved models for SPEs found in MACREE [27] and CHIME [26].

In CRÈME96 [25] the SPE models were replaced with three worst-case models based on

measurements of the October, 1989 SPEs. The worst-week model is based on 180 hours of data during the period 19-27 October. The worst-day model comes from an 18 hour interval of data taken on 20-21 October. The peak flux model is based on the highest 5-minute average proton flux on 20 October and a scaling of the "worst-day" heavy ion fluxes using proton data. All of these models have been shown to be worst-case at the ~99% confidence level [57]. It is important to note [57] that the CRÈME96 SPE models are based on data in the relevant energy range, unlike MACREE and the model of Croley and co-workers [58]. The CRÈME96 SPE models are much more severe than those in CHIME so that SEU rates calculated with the CRÈME96 SPE models are significantly higher. Finally, the CRÈME96 model takes into account the effect of the ionic charge states of SPE heavy ions on geomagnetic transmission to low Earth orbits. For devices in a 28.5° orbit that have a high SEU threshold, the effect of taking into account the ionic charge states (as opposed to assuming the SEPs are bare atomic nuclei) can increase the predicted SEU rate by more than an order of magnitude.

Like Space Radiation, SPENVIS [59] offers a selection of SPE models for use in error rate predictions including the following long-term models: the King Model [54], the JPL Model [51], the Xapsos Models [60]-[62] and a revision of the JPL Model by Rosenqvist and co-workers [63]. The following short-term SPE flux models are also provided, the CRÈME86 [15] and CRÈME96 [25], [57] models and the Xapsos Model [64]

The OMERE model [30] offers a large variety of SPE models both for peak flux and mission integrated fluence. These include SOLPRO [53], ESP [61], CRÈME86 [8] CRÈME96 [25], and JPL91 [51]. OMERE has extended the JPL91 model from 0.5 to 100 MeV using an exponential function. OMERE also offers several models they have developed. These are SPOF (Solar Proton ONERA Fluence) [65], IOFLAR [66] (which fits the spectra of all the elements

with a power law in energy), a worst case flux model based on IMP8 [67] and GOES [68] measurements form 1974 to 2002 and a series of models of individual large SPEs that occurred between 1972 and 2003.

2.3 Geomagnetic Cutoff Transmission

To reach satellites orbiting the Earth within the Earth's magnetosphere, the energetic charged particles in the local interplanetary medium must penetrate the Earth's magnetic field. The ability of a charged particle to penetrate a magnetic field is determined by its magnetic rigidity (or momentum per unit charge). Those particles with magnetic rigidities below the geomagnetic cutoff rigidity will be turned away by the Earth's field before they can reach the satellite.

Access to any point within the magnetosphere can be estimated using the Störmer equation [69] which gives the value of the approximate geomagnetic cutoff, P_c (in GeV/ec), for any location and arrival direction. It is derived under the assumption that the Earth's magnetic field is an ideal dipole. This equation is:

$$P_c = \frac{59.6}{r^2}\left[1 - \left(1 - \cos\theta\cos^3\lambda\right)^{1/2}\right]^2 / \left(\cos\theta\cos\lambda\right)^2$$

where λ is the geomagnetic latitude in offset dipole coordinates, θ is the arrival direction of the particle measured from local East and r is the distance from the offset dipole center in Earth radii. Examination of the Störmer equation reveals that positively charged particles can arrive with lower rigidities from the west. In fact they can arrive (with the right rigidities) up to 50° below the horizon. For the purposes of error rate prediction, it is customary to use the cutoff for particles arriving from the zenith because it is roughly the average cutoff.

The Earth's magnetic field is not a perfect dipole. It has two main components, one

generated in the core of the Earth and a second from currents in the magnetosphere. The internal field is described by the International Geomagnetic Reference Field (IGRF) [70] which changes on time scales of ~10 years, and the external field is described by Tsyganenko magnetospheric field model [71] which changes rapidly with solar activity. Finding the geomagnetic cutoff for any location and arrival direction requires a computer simulation in which a positively charged particle arriving from beyond the magnetosphere is simulated by a negatively charged particle traveling out of the magnetosphere. This negative particle must be launched with a specific rigidity and direction from the location being investigated then followed to determine if it escapes to deep space. Such calculations have been carried out by Shea and Smart [72], [73].

CRÈME86 [11] calculates the orbit-averaged vertical cutoff for a satellite using a precise world-wide grid of vertical cutoffs at an altitude of 20 km that were calculated by ray-tracing [72] as described above. The cutoffs from this grid were interpolated to intermediate points within the grid and to the altitude of the satellite using the Störmer equation, normalized to the four nearest grid points. The cutoff calculations were then averaged along the two-day orbital path to obtain the orbit-averaged geomagnetic cutoff transmission function.

These calculations were then corrected for the shadow that the Earth casts on the satellite (since the Earth blocks the cosmic rays) and for the suppression of the cutoff during large geomagnetic storms. These storms increase the ring current which has the effect of partially cancelling the Earth's field, thus reducing the cutoff.

The NOVICE code [19] uses the CRÈME86 procedure for geomagnetic shielding. MACREE [27] also uses the geomagnetic transmission function from CRÈME86. CHIME [26] simply calculates the geomagnetic cutoff transmission function using the Störmer equation [69] for an offset and tilted dipole fit to the Earth's field. OMERE [30] also uses the Störmer

equation. Space Radiation [20] does an exact calculation of geomagnetic shielding by detailed ray-tracing.

For CRÈME96, a new geomagnetic cutoff ray-tracing calculation was performed [25] using both the updated IGRF [70] and the external field is described by the Tsyganenko magnetospheric field model [71]. Unfortunately, the support for CRÈME96 ended before a world-wide grid using these new calculations could be completed. Calculations for only two orbits; a typical International Space Station orbit (51.6° by 450 km, circular) and a typical Space Shuttle orbit (28.5° at 450 km, circular) were finished. The geomagnetic cutoff transmission to other orbits are calculated using the method of CRÈME86 with interpolating/extrapolating from a more recent ray-tracing calculation of the world-wide cutoff grid based on the geomagnetic field as it was in 1980. Since CRÈME96 was completed work on a vertical cutoff rigidity interpolation tool has been finished [73]. It is based on a 5 by 5 world-wide grid at 450 km calculated by ray-tracing in the combined IGRF and Tsyganenko fields.

SPENVIS [59] uses the Magnetocosmics [74] application, based on GEANT4, for simulating the propagation of cosmic rays through the Earth's magnetic field. It uses a magnetic field model that includes the IGRF along with the user's choice of three Tsyganenko models [71], [75]-[78].

2.4 Trapped Radiation

In addition to the radiation coming from outside, energetic charged particles trapped in the Earth's radiation belt are capable of producing single event effects. The dominant component for single event effects is protons which are principally due to cosmic ray neutron albedo decay [79]. The radiation belt also contains electrons and a small population of low-energy heavy ions,

He, O, Ne, Ar, etc. that come from anomalous cosmic rays that are stripped of their orbital electrons in the upper reaches of the Earth's atmosphere [80], [81]. Electrons are not effective in producing single event effects. The heavier ions make a contribution to the radiation environment only under light shielding as shown in figure 5 of reference [7].

Charged particles trapped in the radiation belt gyrate around a guiding center magnetic field line in the Earth's dipole magnetic field. As a particle approaches one of the magnetic poles, the magnetic field lines converge causing the pitch angle of the particle to rotate to 90° and then beyond causing the particle to spiral back toward the other magnetic pole. This is called mirroring. Particles are thus trapped between their mirror points. The altitude of a particle's mirror points is determined by its pitch angle at the geomagnetic equator. Particles with the smallest equatorial pitch angle will have the lowest mirror point altitudes (particles with lower mirror points are removed by the atmosphere). A result of this is that satellites orbiting at low altitudes experience a higher flux of protons coming from the west because such protons are gyrating about a guiding center field line above the satellite's altitude and experience less atmospheric loss than protons striking the satellite from the east (because they are gyrating around a field line that is below the satellite).

In addition to gyrating around their guiding center field line and bouncing between their mirror points, trapped particles drift around the Earth. This is because as they circle their guiding center field line, the field is a little weaker at the furthest point from the Earth and a little stronger at the nearest point. This causes the particles to execute cycloidal rather than circular motion as they gyrate causing protons to drift westward around the Earth.

The Earth's magnetic field dipole axis is tilted at ~11° relative to the Earth's spin axis and the center of the dipole is offset by ~550 km toward the north Pacific with the result that the

Earth “sticks up” farther into the dipole magnetic field pattern in the south Atlantic than elsewhere. As trapped particles drift over the south Atlantic those with the lowest mirror points encounter the atmosphere and are lost. This is where the lower edge of the radiation belt is defined. While satellites in low-Earth orbit can pass below the radiation belt at other locations around the Earth, they must enter it over the south Atlantic, a region called the South Atlantic Anomaly.

During the active phase of the solar cycle (called solar maximum), the Sun emits more x-rays, heating the upper atmosphere and causing its scale height to increase. This pushes the atmosphere farther up into the radiation belt at solar maximum increasing loss rates of trapped particles with low mirror points. This results in fewer trapped protons being encountered by satellites in low-Earth orbit during the maximum of the solar cycle.

The most widely used model for trapped protons is the AP8 Model [82] (also see [31] for more details of the AP-8 Model). This model is being updated to create AP-9. The expected release date for AP-9 is November, 2011. In addition to these models there are the following models: CRRESPRO [83], the SAMPEX/PET model [84] and NOAAPRO model [85].

Trapped protons are introduced into CRÈME86 [8] using the STASS subroutine. The user is expected to obtain orbit-averaged trapped proton data in the form of a differential spectrum in units of protons/(cm^2-s-KeV) versus proton energy in MeV. Under control of the STASS program, this spectrum table is to be entered as pairs of energy and flux with the energy monotonically increasing. This input table can be generated, for example, using SPENVIS [59]. SPENVIS offers the AP-8 MIN and MAX, CRRESPRO, and the SAMPEX/PET models. Space Radiation [20] also uses an imported trapped proton spectrum. CRÈME96 [25], NOVICE [19] and OMERE [30] use AP-8 for trapped protons. The CHIME model [26] and the MACREE

model [27] do not include trapped radiation.

2.5 Radiation Transport through Shielding

To reach the device of interest within the spacecraft, the radiation must penetrate the surrounding spacecraft structure. When charged particles pass through the structure, they lose energy through interactions with atomic electrons and through nuclear interactions. Since interactions with electrons are so frequent, they can be treated as a continuous process. Nuclear interactions are infrequent and must be treated as individual events. These interactions can be elastic collisions in which some energy is lost through the momentum transfer to a nucleus in the structure, but the projectile nucleus remains intact. Other interactions are inelastic. These interactions increase the internal energy in the projectile nucleus and/or the target nucleus. Nuclei can lose internal energy in a variety of ways. Many of these ways involve the emission of neutrons but charged particles can also be emitted. This changes elemental or isotopic identities of the incident nuclei. As a result of such interactions, the projectile nuclei can even break up into much lighter nuclei and nucleons.

The net effect on radiation penetrating spacecraft is for it to lose energy with the slowest energy particles stopping before reaching the device of interest. The elemental composition of the flux is also altered by the breakup of nuclei reducing the fluxes of the most abundant heavy nuclei while the fluxes lighter and less abundant nuclei are increased by the breakup of heavier progenitors. A rough rule of thumb is that the error rates decrease by a factor of 10 behind 6.5 inches of aluminum shielding [86].

The thickness of the spacecraft surrounding the device of interest is rarely uniform with the result that the intensity and elemental composition of the radiation striking the device from

different directions will be different. This detail is usually ignored in error rate prediction, and the average intensity and composition is assumed to arrive uniformly from all directions. This can lead to significant errors [87], [88], especially when the radiation environment is dominated by SPEs [16].

CHIME [26] makes the "straight ahead" approximation, assuming that particles continue along the same path as they pass through the satellite. It accounts for energy loss through interactions with orbital electrons in the spacecraft structure (i.e. dE/dx loss) but neglects nuclear interactions. CRÈME86 [15] also uses the "straight ahead" approximation and accounts for dE/dx loss but also includes particle losses due to deep inelastic nuclear interactions that fragmented the incident particles. Secondary production in these nuclear interactions is ignored. This is not a serious error for light spacecraft, but becomes more important for heavier spacecraft like the International Space Station. OMERE [30] uses the CRÈME86 algorithm for radiation transport through shielding.

CRÈME96 [25] also uses the "straight ahead" approximation. Unlike CRÈME86, it keeps track of charged nuclear fragments coming from the projectile nuclei. It allows the user to choose a uniform shielding thickness or import a distribution of shielding thicknesses (determined from a sector shielding analysis using other software). CRÈME96 does not track secondary neutrons or fragments of the target nuclei.

Space Radiation [20] offers a variety of ray-tracing routines to transport the external radiation environment to a device within a hollow or solid body having the shape of a sphere, cylinder or box. The location of the device and the dimensions of the shielding are user-specified.

NOVICE offers two methods for shielding calculations [89]. One method divides the 4π

solid angle surrounding the device into solid angle sectors and uses ray-tracing to find both the total and the minimum thickness of the shielding in each sector. The effect of the shielding thickness is then determined by interpolating in a pre-calculated table of environments within spherical shells having a range of thicknesses. The second method is to use an adjoint Monte Carlo to calculate the transport of the external radiation environment to the device. This includes the transport of neutrons and gamma rays. NOVICE also includes a tool to weight-optimize the shield distribution.

SPENVIS offers three solutions to radiation transport through spacecraft. Since SPENVIS includes CRÈME86, the CRÈME86 method described above is available. In addition, two Monte Carlo approaches are offered. Both transport all the particles supported by GEANT4 (GEometry ANd Tracking 4) [90], which now includes neutrons and protons as well as light and heavy ions. The propagation calculations use Monte Carlo methods and can make use of all the physics lists available in GEANT4. MULASSIS (MUlti-LAyered Shielding SImulation Software) [91] allows the user to describe the spacecraft in terms of user-defined layered shields that can be either planar or spherical. GRAS (Geant4 Radiation Analysis for Space) [92] has no restrictions on how the spacecraft structure can be described. The user can construct a description of the spacecraft structure using GEANT4 primitive shapes (e.g. spheres, boxes, cylinders, pyramids, etc.) or the structure can be described in GDML (Geometry Description Markup Language).

3.0 Error Rate Prediction

Precise prediction of the single event effect rates, resulting from known fluxes of particles striking a device, requires detailed and accurate physical descriptions of the individual

interactions of a large sample of particles within the device. Using currently available computers, such an approach is too computationally intensive for a practical engineering design tool. Fortunately, simple models of the interaction process can provide sufficiently accurate error rate predictions in many kinds of devices and in many types of device technologies. This section will describe the transient effects that single ionizing particles can have on electronic circuits, the details of how the particle interacts with the circuit and the models that have been used for error rate prediction.

3.1 Single Event Effects

The list of single event effects grows every year as microelectronics evolves and new effects are discovered. The current list, known to this author, is given below.

Non-destructive single event effects are ones in which the functionality of the circuit can be recovered. They are:

1) Single event transient (SET): This is a radiation-induced current or voltage pulse occurring at a circuit node or the output of an IC. It is caused by a single particle and it may or may not result in an error.
2) Single event upset (SEU) A SEU is a radiation-induced change in a circuit's static logic state. It is one possible outcome of an SET in a specific sensitive circuit node.
3) Single event functional interrupt (SEFI): A SEFI is typically seen as a large burst of errors due to a single ion strike that corrupts control or mode circuitry. It can be self-restoring or it may require reset, or restart.
4) Single Event Latchup (SEL): A SEL occurs when the spurious current transient due to the ionization of a single particle activates one of a pair of parasitic transistors in a CMOS circuit. This pair forms a circuit that shorts the power supply for the device. If the current drawn by

the device is externally limited at a sufficiently low value, the device will not be damaged however power to the device must be cycled to restore its functionality.

5) Multi-Cell Upset (MCU): This occurs when a single ion upsets more than one memory cell.
6) Multi-Bit Upset (MBU): This occurs where an MCU occurs in one word.

There are also destructive single event effects: Single Event Gate Rupture (SEGR), Single Hard Error (SHE), Single Event Burnout (SEB), Single Event Snapback (SES) and Single Event Dielectric Rupture (SEDR). Since this paper is concerned with error rate prediction, destructive single event effects will not be addressed here. The most common non-destructive SEEs begin as SETs. The way SETs develop is described below.

3.2 Time History of a Single Event Transient

The charge collection process has been described in the literature, see [93], [94]. To appreciate the complexity, a detailed physical description of SET development must be given. The speed of light is 300 nanometers/femtosecond so, for example, a 10 MeV/nuc particle will traverse a 65nm feature in 1.5 femtoseconds. In general, the ionizing particle creates its track across the sensitive region of a circuit in <10 femtoseconds. By comparison, the response time of the circuit is on the picosecond scale [93] so for discussions of SETs, we can assume the ionized track appears instantly.

The ionized track left by the particle consists of equal numbers of electrons and holes. The density of ionization falls rapidly from the core of the track outward [95]-[97]. This is shown graphically by Dodd [98] in figure 6 of his paper. For particles that produce sufficient ionization to cause errors, the density of holes and electrons in the core of the track exceeds the background density due to doping in the material. Any pre-existing electric field in the core of

the track will be cancelled by polarization of this hole-electron cloud. This dramatically alters the field configuration in the vicinity of the track. It can, for example, temporarily extend the depth of the depletion region in a reverse biased junction [98]. The electric field still exists in the fringes of the track so charge liberated by the passage of the particle can be collected by drift.

During the first part of the event, charge from the fringes of the track is collected and the core of the track spreads by ambipolar diffusion. This allows the electric field to penetrate deeper into the ionization track so that charge starts to be collected by drift at a higher rate. Diffusion can also play a role in charge collection through the diffusion of charge from a field-free region into one where drift can collect it. This process continues as the track spreads and the electric field penetrates deeper collecting more charge until the ionization track disappears and the electric field returns to its pre-strike configuration.

Describing this mathematically is challenging. The holes and electrons in the core of track are not merely test particles. Their presence alters the conditions under which charge is collected and these conditions continue to change as the event unfolds. The solution to the problem of charge collection requires numerical methods [99]. Such methods are available in various Technology Computer-Aided Design (TCAD) programs [100]-[104].

The calculations are time-consuming because they require gridding the volume of the circuit affected by the track with a 3D tessellation and solving the equations governing drift and diffusion [98], [99] in each volumetric picture element (or voxel) and in small time steps. At the event evolves the ionization track spreads, making it necessary to adaptive gridding [105]. The result of this calculation is a time history of the current collected on each affected node in the circuit. To find out how the circuit will respond to the current transients on the affected nodes, the TCAD program must couple this calculation with a SPICE (Simulation Program with

Integrated Circuit Emphasis) calculation [106], [107]. These coupled model calculations will give an accurate description of the SET and predict its effect, e.g. a SEU. Unfortunately, they are too computationally intensive to be used for error rate prediction [98], [108]. The solution is to adopt a simplified model of charge collection that permits rapid calculation of error rates.

3.3 Methods of Predicting Single Event Effects

Over the 36 years since single event upsets were discovered [1], several techniques have been developed to estimate single event error rates. These techniques have evolved as knowledge was gained from accelerator experiments and experience was gained from applying these techniques to spacecraft data.

3.3.1 Early Approaches

In their calculations, Binder, Smith and Holman [1] used the cosmic ray iron spectrum and took spacecraft shielding into account. They used circuit models to calculate the minimum charge required to cause an error and verified their result using a scanning electron microscope. They then estimated the error rate by calculating the rate at which iron nuclei would deposit the minimum charge required to produce an error. These are still the basic steps required for error rate prediction.

Pickel and Blandford in their 1978 paper [4] investigated SEUs in NMOS dynamic RAMs (DRAMs). They identified the depletion region under the p-n junction as the sensitive volume and represented it with a rectangular parallelepiped. The critical charge, Q_c, required to change the logic state of one of the DRAM cells was estimated. Particles capable of causing an

upset were required to deposit $Emin = 22.5Q_c/f$ (where f is the charge collection efficiency).

This could be the total energy of a particle stopping in the sensitive volume or a particle having a dE/dx such that $SdE/dx2E_{min}$, where S is the average pathlength though the parallelepiped.

3.3.2 Rectangular Parallelepiped Model

The Rectangular ParallelePiped (RPP) model was introduced by Bradford [3], [2] and independently by Pickel and Blandford [5]. In this method the LET spectrum is integrated over the chord length distribution for a rectangular parallelepiped from a threshold LET to the maximum LET in the LET spectrum. The threshold is $LET_0 = 22.5Q_{crit}$ where Q_{crit} is the minimum charge that must be deposited in the sensitive volume to create an upset. The integral over the chord length distribution and LET spectrum according to [16] is,

$$N_e = 22.5\pi AQ_{crit}\int_{\frac{22.5Q_{crit}}{P_{max}}}^{L_{max}} \frac{1}{L^2} D[p(L)]F(L)dL$$

where,

A is the surface area of the sensitive volume in m^2, Q_{crit} is in pC,

$L_{max} = 1.05X10^3 MeV.cm^2/g$ (the largest possible LET), P_{max} is the largest diameter of the sensitive volume in g/cm^2, L is the LET in $MeV.cm^2/g$, $F(L)$ is the integral LET spectrum in particles/m^2.ster.sec and $D[p(L)]$ is the differential chord length distribution of the sensitive volume in cm^2/g where $p(L) = 22.5Q_{crit}/L$ is the pathlength of an ion, with an LET of L, that is

needed to produce a charge, Q_{crit}. There are many equivalent expressions for this integral, some integrating over pathlength [5], others integrating over an integral pathlength distribution and a differential LET spectrum [3], [2]. All these formulations are equivalent.

It was soon recognized that ionization outside the depletion region of a junction could contribute charge to the upset process by diffusing into the junction [2]. It was also discovered that the intense ionization in a charged particle track can distort the electric field in a junction creating a 'field-funneling effect' [109], [110]. These effects can be accommodated within the RPP model by simply extending the depth of the sensitive volume into the substrate below the junction. This was taken into account explicitly in the CRUP program [17]. The RPP method is used in CRÈME86 [15] MACREE [27] and CHIME [26]. CRÈME86 is available on line at https://creme.isde.vanderbilt.edu/ and http://www.spenvis.oma.be/help.php. The RPP method is also available in the commercial software packages, NOVICE [19] and Space Radiation [20].

The RPP model forms the basis for a convenient way to compare the SEU vulnerability of parts. Petersen, Langworthy and Diehl [18] proposed a single event Figure of Merit (FoM) as a guide to choosing devices and as an indicator of the severity of the SEU problem. The FoM provides a comparison of the SEU rates of parts in the 10% environment shown as the chain-dot curve in figure 1. Because of the shape of this LET spectrum, it is possible to fit it with a simple power law. The derivative of this power law with respect to LET is $\phi = 5.8x10^{8}L^{-3}$, where ϕ is the LET flux in particles/cm^2.day.MeV.cm^2/g and L is LET in MeV.cm^2/g. This is a reasonable fit from 20 to 2x10^4 MeV.cm^2/g. Above and below this range; the power law fit overestimates the flux. It should be noted that when the SEU rate is below 10^{-8} upsets/day, it will be overestimated. Under the assumption that the lateral dimensions of the sensitive volume are at

least three times larger than its depth, the estimated error rate, *R* (in upsets per cell-day), becomes

$$R = 5x10^{-10}\sigma_L/L_c^2,$$

where σ_L is the experimentally-determined SEU cross section in μm^2 and L_c is the linear charge deposition threshold for upsets in pC/μm. This equation was restated in [28] with L_c defined as the value of L at 25% of the limiting SEU cross section and the scale constant modified to the obtain,

$$R = 2x10^{-10}\sigma_L/L_{0.25}^2,$$

This modified FoM is presented in other and perhaps more convenient forms in [29]. In [111] Petersen discusses its applicability to many practical situations. He shows that the modified FoM can be adjusted to fit a more exact estimate of the error rate for a soft part and used to estimate error rates in other parts in the same environment. Peterson [86] has shown that the FoM can also be estimated from the limiting cross section for upsets caused by nuclear reactions caused by proton interactions, σ_{PL}, $R = C4.5x10^{-5}\sigma_{PL}$, where C is a constant that varies with the radiation environment.

3.3.3 Effective Flux Model

If the sensitive volume can be modeled as a thin rectangular parallelepiped and the upset cross section rises rapidly to its limiting value just above the upset threshold (i.e. has the form of a Heaviside step function) then the flux capable of causing an upset, ϕ_s, can be

calculated in two terms [21]. The first is $\phi_e(L) = \phi(L)(L/L_c)^2/2$ when $L < L_c$, where ϕ and ϕ_e are the differential LET spectra, L is LET and L_c is the threshold LET for producing an upset at normal incidence. The second term is $\phi_e(L) = \phi(L)/2$ when $L \geq L_c$. This model was implemented in the SEFA model [22].

3.3.4 IRPP Model

From accelerator measurements of SEU cross sections versus LET, it soon became apparent [18] that SEU cross sections do not always rise rapidly to their limiting values just above the LET threshold. Several reasons were suggested for this effect [18], [23], [111]. It has been suggested that the gradually increasing threshold is due to process variations on across the die causing parameters to vary from cell to cell [23], that two or more sensitive volumes in a memory cell have different thresholds or that the sensitivity varies across the sensitive volume [112], [113]. For a more in-depth discussion of the causes for the gradual increase of the cross section see [111] and [114].

(Insert figure 4 here)

The solid curve in figure 4 is a model of a typical SEU cross section curve. To conceive how to calculate the error rate from such a cross section curve, one can think of representing the cross section in a series of steps at successively higher LET values, as shown by the dashed lines in figure 4. The RPP model can then be used to calculate the partial SEU rate for each step, as is done in CHIME [26].

The logical extension of this approach is to integrate the RPP model over the cross section curve [23], [115], [116], [111]. The first step is to normalize the cross section curve to the maximum cross section and fit it with an analytic representation. The preferred representation

is the integral form of the Weibull Distribution [23].

$$F(L) = 1 - \exp\left\{-\left[\left(L - \frac{L_0}{W}\right]^S\right\} \qquad L > 0$$

$$= 0 \qquad L \leq 0$$

Where L_0 is the LET threshold, W is width and S is the shape parameter of the distribution.

Petersen [86] shows that $L_{0.23}$ in the modified FoM formula (above) can be derived from the Weibull fit parameters, i.e. $L_{0.23} = L_0 + W[0.286]^{1/S}$.

The error rate estimate, N, then becomes [111],

$$N = \frac{S}{4}\int_{L_0}^{L_{max}} f(L_W) \int_{L_0}^{L_{max}} \Phi(L) D\left(\frac{cL_W}{L}\right) dL\, dL_W$$

Where S is the surface area of the sensitive volume, $f(L_W)$ is the differential Weibull Distribution, L_{max} is the maximum LET in the LET spectrum, L_0 is the threshold LET measured with the accelerator beam normally incident on the device. L_W and L are variables of integration, $\Phi(L)$ is the differential LET spectrum and $D\left(\frac{cL_W}{L}\right)$ is the integral chord length distribution of the sensitive volume where c is the depth of the sensitive volume. For a more in-depth discussion of the IRPP model and related topics, see [111] and [114].

IRPP model has been implemented in CRÈME96 [25], the CHIME model [26], the Heavy Ion Cross Section for Single Event Upset (HICUP) model [115], [116] and OMERE [30]. It is also used in Space Radiation [20].

3.5 Best Practices for Error Rate Prediction with the RPP and the IRPP methods

The first step is to decide what approach to take. For the RPP model, the following conditions [108] must be satisfied:

i) A single rectangular parallelepiped can be used to represent the sensitive volume associated the occurrence of a transient single event effect.

ii) The probability of occurrence of an SEE is determined entirely by the total energy deposited, E_d, in the sensitive volume.

iii) The deposited energy is completely determined by the product of the LET (which is assumed to be constant within the sensitive volume) and the length of particle's track crossing the sensitive volume.

iv) The SEE occurs if and only if the E_d exceeds the critical energy needed to cause the SEE. That is to say that the SEE cross section has the form of a Heaviside Step Function, increasing abruptly to its limiting value.

Some of the tools for error rate prediction [19], [20], [27], [30], [59] do not hold LET constant across the sensitive volume but account changes in LET within the sensitive volume. This is important for low energy particles and large devices like optocouplers and CCDs [117], [118]. Condition iv) can be relaxed if the IRPP approach is used. By integrating over the shape of the normalized SEE cross section, it possible to deal with the cases where there is a known probability (but not a certainty) that a SEE will occur if E_d exceeds the critical energy.

The IRPP approach as it is implemented in CREME96 and the other tools is still the best choice for error rate prediction on most currently available electronic devices. For those devices that do not meet the conditions for use of the IRPP method, the newly developed Monte Carlo approach [108], CRÈME-MC (available at https://creme.isde.vanderbilt.edu/) can be used.

For detailed advice on the best way to make SEE rate predictions using the IRPP model, the reader is referred to the following references [23], [111], [114], [122], [117], [119] and [127]. Also see [28], [29], [88], [120], [121], [123], [124], [125], [126] and [128]

3.6 Proton- and Neutron-Induced SEEs

Protons and neutrons can cause SEEs indirectly by initiating nuclear interactions in or near the sensitive volume [129], [130]. In very soft devices or ones with large sensitive volumes (e.g. CCD arrays) protons can also cause SEEs by direct ionization. The error rate for SEEs caused in this way can be estimated using the RPP, IRPP or Monte Carlo methods discussed above. This section will focus on SEEs resulting from nuclear interactions.

Approximately 1 in 10^5 protons passing through the device will cause a nuclear reaction that deposits enough energy in the sensitive volume to cause an SEE. The abundance of heavier ions in cosmic rays and SEPs is $\geq 1\%$ so SEEs caused indirectly by protons are not important, but the composition of radiation trapped in the Earth's magnetic field is practically pure protons except at low energies where trapped anomalous cosmic rays contribute heavy ion content. Also, the flux of trapped protons in the inner radiation belt is so high that SEEs due to proton-induced nuclear reactions dominate those caused by heavy ions entering the magnetosphere from the interplanetary medium.

This problem of estimating error rates caused by proton-induced nuclear reactions was first addressed by investigating the nuclear cross sections in silicon that can produces SEEs. Both analytic and Monte Carlo methods were used. For further discussion of these approaches, the reader is referred to [111]. An empirical approach is commonly used to estimate these error rates. The first such approach was presented by Bendel and Petersen [131]. Combining

theoretical knowledge of the behavior of proton-induced reactions near threshold and at high energies with fits to measured SEU cross sections, the authors obtained the Bendel One-Parameter Model, for the upset cross section, σ, in units of upsets per proton/cm^2.bit,

$$\sigma = (24/A)^{14}[1 - \exp(-0.18Y^{0.8}]^4 \text{ and } Y = (18/A)^{0.8}(E - A),$$

where A is a free parameter (in MeV) that must be fitted to experimental data for the device at some energy, and E is the proton energy in MeV. Once fitted, this cross section must be combined with the proton spectrum at the part to obtain the SEU rate.

The Bendel Model was later improved [132] by adding a second parameter to obtain,

$$\sigma = (B/A)^{14}[1 - \exp(-0.18Y^{0.8}]^4$$

Petersen [111] recommends replacing this form with a log-normal form of the cross section when sufficient data exist to be fitted. Another approach, implemented in CRÈME96 [25], is to fit the cross section data with a Weibull distribution.

CRÈME89 offers the One Parameter Bendel Model which is also included in MACREE [27] and NOVICE [19]. CRÈME96 offers the one and two parameter Bendel models as well as Weibull fits to proton-induced SEU cross sections. OMERE [30] offers these models plus the PROFIT [133] and SIMPA [134] models. The OMERE model is also used in SPENVIS. Space Radiation [20] offers the one and two parameter Bendel models and Weibull fits to proton-induced SEU cross sections. It also makes use of Peterson's relationship between the FoM and the limiting cross section for upsets [86]. In addition it offers a Monte Carlo calculation of proton interactions in the chip using fundamental nuclear cross section data. The CUPID code [135] uses Monte Carlo methods to estimate error rates due to nuclear reaction caused by protons.

Neutrons are generated in spacecraft and in the atmosphere by the interactions of cosmic

rays and SEPs. For satellites in low Earth orbit, the neutron flux is a combination of locally generated neutrons and neutron albedo from the atmosphere. There is also neutron albedo from the surface of the Moon that affects electronics on or near the lunar surface. Like protons, neutrons can produce SEEs by causing nuclear reactions. The methods for calculating neutron-induced SEUs include the burst generation rate approach [136] and Monte Carlo simulations [137]. Normand [138] has shown that the proton limiting cross section, σ_{PL}, can be used to obtain and estimate of the SEU rate for neutrons. Normand report that the neutron-induced SEU rate at 40,000 ft and 45 degrees latitude is $R_n = 6000\sigma_{PL}$, or using Petersen's FoM, he obtains

$$R_n = 3.2FoM.$$

For detailed advice on the best way to make SEE rate predictions of proton- and neutron-induced SEEs, see [111], [114] and [138].

4.0 Conclusions

This chapter has reviewed CRÈME96 and related error rate prediction methods. These methods are not applicable some of the newest components, but they can be used to predict error rates most of components in use today. The models for obtaining the environment at the components within spacecraft will remain applicable for the foreseeable future, though improvements are needed in several aspects. Work on these models continues.

The SEP models are being extended to probabilistic models that provide differential energy spectra for all the elements for the peak flux as well as the event-integrated fluence and mission-integrated fluence. Also the AP-9 model is nearing completion and will soon be added to the existing codes. The available radiation environment models, which principally apply to

conditions near Earth, are being extended to other destinations in the heliosphere. It will be some years before this work is completed.

References:

[1] D. Binder, E. C. Smith, and A. B. Holman, "Satellite Anomalies from Galactic Cosmic Rays," *IEEE Transactions on Nuclear Science,* vol. 22, no. 6, pp. 2675-2680, 1975.

[2] J. N. Bradford, "Geometrical Analysis of Soft Errors and Oxide Damage Produced by Heavy Cosmic Rays and Alpha Particles," *IEEE Transactions on Nuclear Science,* vol. 27, no. 1, pp. 942-947, 1980.

[3] J. N. Bradford, "A distribution function for ion track lengths in rectangular Volumes," *J. Appl. Phys.*, Vol. 50. No. 6, pp. 3799-3801, 1979.

[4] J. C. Pickel and J. T. Blandford, Jr., "Cosmic Ray Induced Errors in MOS Memory Cells," *IEEE Transactions on Nuclear Science,* vol. 25, no. 6, pp. 1166-1171, 1978.

[5] J. C. Pickel and J. T. Blandford, Jr., "Cosmic-Ray-Induced Errors in MOS Devices," *IEEE Transactions on Nuclear Science,* vol. 27, no. 2, pp. 1006-1015, 1980.

[6] W. Heinrich, "Calculation of LET-Spectra of Heavy Cosmic Ray Nuclei at Various Absorber Depths," *Radiation Effects* vol. 34, pp. 143-148, 1977.

[7] J. H. Adams, Jr., "The Natural Radiation Environment inside Spacecraft," *IEEE Transactions on Nuclear Science,* vol. 29, no. 6, pp. 2095-2100, 1982.

[8] J. H. Adams, Jr., R. Silberberg, and C. H. Tsao, "Cosmic Ray Effects on Microelectronics, Part I: The Near-Earth Particle Environment," Washington, DC: Naval Research Laboratory, Memorandum Report No. 4506, 1981.

[9] J. H. Adams, Jr., R. Silberberg, and C. H. Tsao, "An Analytical Model for the Differential Energy Spectra of Cosmic Rays," in *Proc. of the 17th Int. Cosmic Ray Conf.* vol. 8, pp. 94-98, 1981.

[10] J. H. Adams, Jr., R. Silberberg, and C. H. Tsao, "Cosmic Ray Effects on

Microelectronics," *IEEE Transactions on Nuclear Science,* vol. 29, no. 1, pp. 169-172, 1982.

[11] J. H. Adams, Jr., J. R. Letaw, and D. F. Smart, "Cosmic Ray Effects on Microelectronics, Part II: The Geomagnetic Cutoff Effects," Washington, DC: Naval Research Laboratory, Memorandum Report No. 5099, 1983.

[12] R. Silberberg, C. H. Tsao, J. H. Adams, Jr., and J. R. Letaw, "LET-Distributions and Radiation Doses Due to Cosmic Rays," *IEEE Transactions on Nuclear Science,* vol. 30, no. 6, pp. 4405-4408, 1983.

[13] J. H. Adams, Jr. and A. Gelman, "The Effects of Solar Flares on Single Event Upset Rates," *IEEE Transactions on Nuclear Science,* vol. 31, no. 6, pp. 1212-1216, 1984.

[14] J. H. Adams, Jr., A. J. Tylka, and B. Stiller, "LET Spectra in Low Earth Orbit," *IEEE Transactions on Nuclear Science,* vol. 33, no. 6, pp. 1385-1389, 1986.

[15] J. H. Adams, Jr., "Cosmic Ray Effects on Microelectonics, Part IV," Washington, DC: Naval Research Laboratory, Memorandum Report No. 5901, 1986.

[16] J. H. Adams, Jr., "Variability of Single Event Upset Rates in the Natural Environment," *IEEE Transactions on Nuclear Science,* vol. 30, no. 6, pp. 4475-4480, 1983.

[17] P. Shapiro, "Calculation of Cosmic Ray Induced Single Event Upsets: Program CRUP, Cosmic Ray Upset program," Washington. DC: Naval Research Laboratory, Memorandum Report No. 5171, 1983.

[18] E.L. Petersen, J.B. Langworthy, and S. E. Diehl, "Suggested Single Event Upset Figure of Merit," *IEEE Transactions on Nuclear Science,* vol. 30, no. 6, pp. 4533-4539, 1983.

[19] T.M. Jordan, *NOVICE.* Experimental and Mathematical Physics Consultants, www.empc.com.

[20] Space Radiation Associates, *Space Radiation.* http://www.spacerad.com.

[21] D. Binder, "Analytic SEU Rate Calculation compared to Space Data," *IEEE Transactions on Nuclear Science,* vol. 35, no. 6, pp. 1570-1572, 1988.

[22] T. M. Scott, "A single Event Rate Calculation Technique," IBM, Report 89-PN6-004*,* 1989.

[23] E. L. Petersen, J. C. Pickel, J. H. Adams, Jr., and E. C. Smith, "Rate Prediction for Single Event Effects – a Critique," *IEEE Transactions on Nuclear Science,* vol. 39, no. 6, pp. 1577-1599, 1992.

[24] J. C. Pickel, "Single Event Effect Rate Prediction," *IEEE Transactions on Nuclear Science,* vol. 43, no. 2, pp. 483-495, 1996.

[25] A. J. Tylka et al., "CRÈME96: A Revision of the Cosmic Ray Effects on Micro-Electronics Code," *IEEE Transactions on Nuclear Science,* vol. 44, No. 6, pp. 2150-2160, 1997.

[26] D. L. Chenette et al., "The CRRES/SPACERAD Heavy Ion Model of the Environment (CHIME) for Cosmic Ray and Solar Particle Effects on Electronic and Biological Systems in Space," *IEEE Transactions on Nuclear Science,* vol. 41, No. 6, pp. 2332-2339, 1994.

[27] P. P. Majewski, E. Normand, and D. L. Oberg, "A New Solar Flare Heavy Ion Model and Its Implementation Through MACREE, An Improved Modeling Tool to Calculate Single Event Effect Rates in Space," *IEEE Transactions on Nuclear Science,* vol. 42, No. 6, 21043-2050, 1995.

[28] E. L. Petersen, J. C. Pickel, E. C. Smith, P. J. Rudeck and J. R Letaw, "Geometrical Factors in SEE Rate Calculations," *IEEE Transactions on Nuclear Science,* vol. 40, No. 6, pp. 1888-1909, 1993.

[29] E. L. Petersen, "SEE Rate Calculations Using The Effective Flux Approach and a Generalized Figure of Merit Approximation," *IEEE Transactions on Nuclear Science,* vol. 42, no. 6, pp. 1995-2003, 1995.

[30] TRAD, "OMERE Software," http://www.trad.fr/OMERE-Software.html.

[31] J. Barth, "Modeling Space Radiation Environments," *Nuclear and Space Radiation Effects Conference Short Course Notes,* July 2007.

[32] E. Anders and N. Grevesse, "Abundances of the elements: Meteoritic and solar," *Geochimica et Cosmochimica Acta*, vol. 53, pp. 197-214, 1989.

[33] B. D. Fields, K. A. Olive, M. Cassé, and E. Vangioni-Flam, "Standard cosmic ray energetics and light element production," *Astronomy and Astrophysics*, vol. 370, pp. 623-634, 2001.

[34] J. C. Higdon and R. E. Lingenfelter, "OB Associations, Supernova-Generated Superbubbles, and the Source of Cosmic Rays," *Ap. J.*, vol. 628, pp. 738–749, 2005.

[35] W. R. Binns, M. E. , "OB Associations, Wolf–Rayet Stars, and the Origin of Galactic Cosmic Rays," *Space Science Reviews*, vol. 130, pp. 439-449, 2007.

[36] J. C. Higdon and R. E. Lingenfelter, "The Myriad-Source Model of Cosmic Rays. I. Steady State Age and Path Length Distributions," *Ap. J.*, vol. 582, pp. 330–341, 2003.

[37] L. J. Gleeson and W. I. Axford, "Solar Modulation of Galactic Cosmic Rays," *Ap. J.,* vol. 154, pp. 1011-1026, 1968.

[38] R.A. Nymmik, M.I. Panasyuk, T. I. Pervaja, and A.A. Suslov, "A Model of Galactic Cosmic Ray Fluxes," *Nucl. Tracks & Radiat. Meas,* vol. 20, pp. 427-429, 1992.

[39] D. Falconer, A. F. Barghouty, I. Khazanov and R. Moore, "A tool for empirical forecasting of major flares, coronal mass ejections, and solar particle events from a proxy of

active-region free magnetic energy," *Space Weather*, vol. 9, S04003, 2011.

[40] R. A. Mewaldt et al., "Proton, helium, and electron spectra during the large solar particle events of October–November 2003," *JGR,* vol. 110, A09S18, 2005.

[41] D. V. Reames, "Magnetic Topology of Impulsive and Gradual Solar Energetic Particle Events," *Ap. J.*, vol. 571, pp. L63–L66, 2002.

[42] A. J. Tylka, "Shock Geometry, Seed Populations, and the Origin of Variable Elemental Composition at High Energies in Large Gradual Solar Particle Events," *Ap. J.*, vol. 625, pp. 474–495, 2005.

[43] L. S. Sollitt, "Ionic Charge States of Solar Energetic Particles," Ph.D. thesis, California Institute of Technology, Pasadena, CA, 2004.

[44] L. S. Sollitt et al., "A Novel Technique to Infer Ionic Charge States of Solar Energetic Particles," *Ap. J.,* vol. 679, pp. 910-919, 2008.

[45] N. V. Nitta, D. V. Reames, M. L. DeRosa, Y. Liu, S Yashiro and N. Gopalswamy, "Solar Sources of Impulsive Solar Energetic Particle Events and their Magnetic Field Connection to Earth," *Ap. J.,* vol. 650, pp. 438-450, 2006.

[46] D. Lario, "Advances in modeling gradual solar energetic particle events," *Adv. in Sp. Res.,* vol. 36, pp. 2279-2288, 2005.

[47] E. N. Parker, "Dynamics of the Interplanetary Gas and Magnetic Fields," *Ap. J.,* vol. 128, pp. 664-676, 1958.

[48] E. C. Roelof, "Propagation of Solar Cosmic Rays in the Interplanetary Magnetic Field," *Lectures in High-Energy Astrophysics*, NASA SP-199. Scientific and Technical Information Division, Office of Technology Utilization, NASA, Washington, D.C., pp. 111, 1969.

[49] M. E. Wiedenbeck, G. M. Mason, C. M. S. Cohen, N. V. Nitta, R. Gómez-Herrero and D. K. Haggerty, "Observations of Broad Longitudinal Extents of 3He-rich SEP Events," *Proc. 32nd Cosmic Ray Conf.,* Beijing: http://icrc2011.ihep.ac.cn/index.htm, 2011.

[50] J. H. Adams, Jr. and A. Gelman, "The Effects of Solar Flares on Single Event Upset Rates", *IEEE Transactions on Nuclear Science,* vol. 31, no. 6, pp. 1212-126, 1984.

[51] J. Feynman, G. Spitale, and J. Wang, "Interplanetary Proton Fluence Model: JPL 1991," *JGR,* vol. 98, no. A8, pp. 13,281-13,294, 1993.

[52] J.A. Simpson, M.G. Munioz, M. Perkins, and J.P. Wefel, "The experiment for high energy nuclei composition (ONR-604)," *CRRES/SPACERAD Experiment Descriptions*, M.S.Gussenhoven, E.G. Mullen. and R.C. Sagalyn eds., Air Force Geophysics Laboratory Report AFGL-TR-85-0017, Hanscom AFB, MA, pp. 163-180, 1985.

[53] E.G. Stassinopoulos, "SOLPRO: A Computer Code to Calculate Probabilistic Energetic Solar Proton Fluences," *NSSDC 75-11,* Greenbelt, Maryland, 1975.

[54] J.H. King, "Solar Proton Fluences for 1977-1983 Space Missions," *J. Spacecraft & Rockets,* vol. 11, pp. 401, 1974.

[55] H.H. Sauer, R.D. Zwickl, and M.J. Ness, "Summary Data for the Solar Energetic Particle Events of August through December 1989," *NOAA Space Environment Laboratory Report*, Boulder, CO, 1990.

[56] T.J. Lie and W.A. Kolasinski, "New Solar Flare Particle Environment Models and Titan/Centaur INU Multiple-Bit Single Event Upset Rates," Aerospace Corporation, El Segundo, CA, Rep. TR-95(5530)-2, 1995.

[57] A. J. Tylka, W. F. Dietrich and P. R. Boberg, "Probability Distributions of High Energy Solar-Heavy-Ion Fluxes from IMP-8: 1973-1996," *IEEE Transactions on Nuclear*

Science, vol. 44, No. 6, pp.2140-2149, 1997.

[58] D.R. Croley, H.B. Garrett, G.B. Murphy, and T.L. Garrard, "Solar Particle Induced Upsets in the TDRS-1 Attitude Control System RAM During the October 1989 Solar Particle Events," *IEEE Transactions on Nuclear Science,* vol. 42, No. 5, pp. 1489-1496, 1995.

[59] SPENVIS, http://www.spenvis.oma.be/intro.php.

[60] M.A., Xapsos, G. P. Summers, J. L. Barth, E. G. Stassinopoulos, and E. A. Burke, "Probability Model for Worst Case Solar Proton Event Fluences," *IEEE Transactions on Nuclear Science,* vol. 46, No. 6, pp. 1481-1485, 1999.

[61] M. A. Xapsos, G. P. Summers, J. L. Barth, E. G. Stassinopoulos, and E. A. Burke, "Probability Model for Cumulative Solar Proton Event Fluences," *IEEE Transactions on Nuclear Science,* vol. 47, No. 3, pp. 486-490, 2000.

[62] M. A. Xapsos, C. Stauffer, T. Jordan, J. L. Barth, and R. A. Mewaldt, "Model for Cumulative Solar Heavy Ion Energy and Linear Energy Transfer Spectra," *IEEE Transactions on Nuclear Science,* vol. 54, No. 6, pp.1985-1989, 2007.

[63] L. Rosenqvist et al., "Toolkit for Updating Interplanetary Proton-Cumulated Fluence Models," *Journal of Spacecraft and Rockets,* vol. 42, No. 6, pp. 1077-1090, 2005.

[64] M. A. Xapsos, R. J. Walters, G. P. Summers, J. L. Barth, E. G. Stassinopoulos, S. R. Messenger, E. A. Burke, "Characterizing solar proton energy spectra for radiation effects applications," *IEEE Transactions on Nuclear Science,* vol. 47, no. 6, pp 2218-2223, 2000.

[65] D. Boscher, S. Bourdarie, D. Lazaro, C. Inguimbert, B. Dirassen, G. Panabiere, "Moyens d'evaluation de l'environnement radiatif des vehicules spatiaux," *Technical report ONERA RTS 2/06923*, Labège, France, 2003.

[66] D. Boscher, S. Bourdarie, C. Inguimbert, B. Dirassen, G. Panabiere, "Moyens d'évaluation

de l'environnement radiatif de vehicules spatiaux," *Report ONERA RTS 2/05726 DESP,* Labège, France, 2001.

[67] K.I. Paularena and J.H. King, "NASA's IMP 8 Spacecraft," *NATO Science Series,* vol. 537, pp. 145-154, 1999.

[68] T. G. Onsager, R. Grubb, J. Kunches, L. Matheson, H. Sauert , D. Speich, and R. Zwickl, "Operational uses of the GOES energetic particle detectors," *SPIE,* vol. 2812, pp. 281-290, 1996.

[69] C. Störmer, "The Polar Aurora," *Clarendon Press,* Oxford, 1955.

[70] T. J. Sabaka, R. A. Langel, R. T. Baldwin and J. A. Conrad, "The geomagnetic field, 1900– 1995, including the large scale fields from magnetospheric sources and NASA candidate models for the 1995 IGRF revision," *J. Geomag. Geoelect.,* vol. 49, pp. 157–206, 1997.

[71] N. A. Tsyganenko, "Determination of magnetospheric current system parameters and development of experimental geomagnetic field models based on data from IMP and HEOS satellites," *Planet. Space Sci.,* vol. 37, pp. 5–20, 1989.

[72] M.E. Shea and D.F. Smart, "Tables of Asymptotic Directions and Vertical Cutoff Rigidities for a Five Degree by Fifteen Degree World Grid as Calculated Using the International Geomagnetic Reference Field for Epoch 1975.0," *AFCRL-TR-75-0185,* Hanscom AFB, MA, 1975.

[73] D.F. Smart, M.A. Shea, A.J. Tylka and P.R. Boberg, "A geomagnetic cutoff rigidity interpolation tool: Accuracy verification and application to space weather," *Adv. Sp. Res.*, vol. 37, pp. 1206-1217, 2006.

[74] L. Desorgher, "Magnetocosmics Software Users Manual," Physikalisches Institut

University of Bern, http://reat.space.qinetiq.com/septimess/magcos/magnetocosmics_sum.pdf, Bern, 2004.

[75] N. A. Tsyganenko, "Modeling the Earth's magnetospheric magnetic field confined within a realistic magnetopause," *JGR,* vol. 100, pp. 5599, 1995.

[76] N. A. Tsyganenko, "Effects of the solar wind conditions on the global magnetospheric configuration as deduced from data-based field models," *Eur. Space Agency Spec. Publ., ESA SP-389,* pp. 181, 1996.

[77] N. A. Tsyganenko, "A model of the near magnetosphere with a dawn-dusk asymmetry, 1. Mathematical structure," *JGR,* vol. 107, JA000219, 2001.

[78] N. A. Tsyganenko, "A model of the near magnetosphere with a dawn-dusk asymmetry, 2. Parameterization and fitting to observations," *JGR,* vol. 107, JA000220, 2001.

[79] A. Dragt, M. M. Austin and R. S. White, "Cosmic Ray and Solar Proton Albedo Neutron Decay Injection," *JGR,* vol. 71, no. 5, pp. 1293-1304, 1966.

[80] J. B. Blake and L. M. Friesen, "A Technique to Determine the Charge State of the Anomalous Low-Energy Cosmic Rays," *Proc. 15th Intl. Cosmic Ray Conf.,* Plovdiv: vol. 2, pp. 341-346, 1977.

[81] N. L. Grigorov et al., "Evidence for trapped anomalous cosmic ray oxygen ions in the inner magnetosphere," *Geophys. Res.Lett.,* vol. 18, no. 11, pp. 1959-1962, 1991.

[82] D. M. Sawyer and J. I. Vette, "AP-8 Trapped Proton Environment for Solar Maximum and Solar Minimum," *National Space Science Data Center/WDC-A-R&S 76-06*, Greenbelt, MD, 1976.

[83] J. D. Meffert and M. S. Gussenhoven, "CRRESPRO Documentation," *Phillips Laboratory PL-TR-94-2218,* Hanscom Air Force Base, MA, 1994.

[84] D. Heynderickx, M. Kruglanski, V. Piercard, J. Lemaire, M.D. Looper and J.B. Blake, "A Low Altitude Trapped Proton Model for Solar Minimum Conditions Based on SAMPEX/PET Data," *IEEE Transactions on Nuclear Science,* vol.46, no. 6, pp. 1475-1480, 1999.

[85] S. L. Huston and K. A. Pfitzer, "A New Model For The Low Altitude Trapped Proton Environment," *IEEE Transactions on Nuclear Science,* vol. 45, No. 6, pp. 2972-2978, 1998.

[86] E. L. Petersen, "The SEU Figure of Merit and Proton Upset Rate Calculations," *IEEE Transactions on Nuclear Science,* vol. 45, No. 6, pp. 2550-2562, 1998.

[87] E. C. Smith, "Effects of Realistic Satellite Shielding on SEE Rates," *IEEE Transactions on Nuclear Science,* vol.41, No. 6, pp. 2396-2399, 1994.

[88] E. L. Petersen, "Predictions and Observations of SEU Rates in Space," *IEEE Transactions on Nuclear Science,* vol.44, No. 6, pp. 2174-2187, 1997.

[89] T. M. Jordan, "Space system analysis using the NOVICE code system," *First European Conference on Radiation and its Effects on Devices and Systems, RADECS 91,* pp. 312-316, 1991.

[90] J. Allison et al., "Geant4 developments and applications," *IEEE Transactions on Nuclear Science,* vol. 53, No. 1, pp. 270-278, 2006.

[91] F. Lei et al., "MULASSIS: A Geant4-Based Multilayered Shielding Simulation Tool," *IEEE Transactions on Nuclear Science*, vol. 49, No. 6, pp. 2788-2793, 2002.

[92] G. Santin, V. Ivanchenko, H. Evans, P. Nieminen and E. Daly, "GRAS: A General-

Purpose 3-D Modular Simulation Tool for Space Environment Effects Analysis," *IEEE Trans. Nucl. Sci.,* vol. 52, No. 6, pp. 2294-2299, 2005.

[93] R. Reed, "Fundamental Mechanisms of Single Particle-Induced Soft Errors", *Nuclear and Space Radiation Effects Conference Short Course Notes,* July 2008.

[94] S. E. Kerns, "Transient-Ionization and Single-Event Phenomena" in *Ionizing Radiation Effects in MOS Devices and Circuits,* T. P. Ma and P. V. Dressendorfer, eds., John Wiley & Sons, New York, 1989.

[95] E. J. Kobetich and R. Katz, "Energy deposition by electron beams and 6 rays," *Phys. Rev.,* Vol. 170, no. 2, pp. 391-396, 1968.

[96] M. P. R. Waligbrski, R. N. Hamm, and R. Katz, "The radial distribution of dose around the path of a heavy ion in liquid water," *Int. J. Radiat. Appl. Instrum. D,* Vol. 11, no. 6, pp. 309-319, 1986.

[97] R. Katz, K. S. Loh, L. Daling, and G. R. Huang, "An analytic representation of the radial distribution of dose from energetic heavy ions in water, Si, LiF, NaI, and SiOz ," *Rad. ESJ: Det Solids,* vol. 114, no. 1, pp. 15-20, 1990.

[98] P. E. Dodd, "Device Simulation of Charge Collection and Single-event Upset", *IEEE Trans. Nucl. Sci.,* vol. 43, No. 2, pp. 561-575, 1996.

[99] P. E. Dodd, "Basic Mechanisms and Modeling of Single-Event Upset in Digital Microelectronics", *IEEE Trans. Nucl. Sci.,* vol. 50, No. 3, pp. 583-602, 2003.

[100] Davinci Three-Dimensional Device Simulation Program Manual: Synopsys, Inc., 2003.

[101] Taurus Process/Device User's Manual: *Synopsys, Inc.*, 2003.

[102] Athena/Atlas User's Manual: *Silvaco Int.*, 1997.

[103] "DESSIS user's manual," *ISE Integrated Systems Engineering AG*, Release 4, vol. 5, 1997.

[104] A. I. Fedoseyev, V. Kolobov, R. Arslanbekov and A. Przekwas, "Kinetic simulation tools for nano-scale semiconductor devices", *Microelectronic Engineering*, Vol. 69, pp. 577–586, 2003.

[105] A. I. Fedoseyev, M. Turowski, M. L. Alles and R. A. Weller, "Accurate numerical models for simulation of radiation events in nano-scale semiconductor devices", *Mathematics and Computers in Simulation*, Vol. 79, pp.1086–1095, 2008.

[106] J. G. Rollins and J. Choma, Jr., "Mixed-mode PISCES-SPICE coupled circuit and device solver," *IEEE. Trans. Computer-Aided Design*, Vol. 7, no. 8, pp. 862-867, 1988.

[107] M. Turowski, A. Raman, and A. I. Fedoseyev, "Mixed-Mode Simulation of Single Event Upsets in Modern SiGe BiCMOS Mixed-Signal Circuits", *MIXDES 2009, 16th International Conference "Mixed Design of Integrated Circuits and Systems"*, pp. 462-467, Lodz, Poland, 2009.

[108] R. A. Weller, R. A. Reed, K. M. Warren, M. H. Mendenhall, B. D. Sierawski, R. D. Schrimpf and L. W. Massengill, "General Framework for Single Event Effects Rate Prediction in Microelectronics", *IEEE Trans. Nucl. Sci.,* vol. 56, No. 6, pp. 3098-3108, 2009.

[109] T. C. May and M. H. Woods, "Alpha-Particle-Induced Soft Errors in Dynamic Memories," *IEEE Trans. Elect. Dev.,* Vol. ED-26, No. 1, 2-9**,** 1979.

[110] C . M. Hsieh, P. C. Murley and R. R. O'Brien, "A Field-funneling Effect on the Collection of Alpha-particle-Generated Carriers in Silicon Devices," *IEEE Elect. Dev. Lett.,* Vol. EDL-2, No. 4, pp. 103-105, 1981.

[111] E. L. Petersen, "Soft Error Results Analysis and Error Rate Prediction," *Nuclear and Space Radiation Effects Conference Short Course Notes,* July 2008.

[112] J. H. Cutchins et al., "Heavy Ion and Proton Analysis of a GaAs C-Higfet SRAM," *IEEE Trans. Nuc. Sci.,* Vol. 40, pp. 1660-1665, 1993.

[113] S. Buchner, J. B. Langworthy, W. J. Stapor, A. B. Campbell, and S. Rivit, "Implications of the Spatial Dependence of the Single-Event-Upset Threshold in SRAMs Measured with a Pulsed Laser," *IEEE Trans. Nuc. Sci.,* Vol. NS-41, No. 6, pp. 2195-2202, 1994.

[114] E. Petersen, *Single Event Effects in Aerospace.* Hoboken, NJ: John Wiley & Sons, 2011

[115] L. W. Connell, P. J. McDaniel, A. K. Prinja, and F. W. Sexton, "Modeling the Heavy Ion Upset Cross Section," *IEEE Trans. Nuc. Sci.,* Vol. 42, No. 2, pp. 73-82, 1995.

[116] L. W. Connell and F. W. Sexton, "Further Development of the Heavy Ion Cross Section for Single Event Upset: Model (HICUP)," *IEEE Trans. Nuc. Sci.,* Vol. 42, No. 6, pp. 2026-2034, 1995.

[117] P. W. Marshall, "Rate Prediction Tool Assessment for Single Event Transient Errors on Optical Link Receivers and Optocouplers", http://radhome.gsfc.nasa.gov/radhome/papers/OptoToolAssmt_032802.pdf, 2002.

[118] A. H. Johnston, G. M. Swift, T. Miyahira, S. Guertin and L. D. Edmonds, "Single-Event Upset Effects in Optocouplers," *IEEE Trans. Nuc. Sci.,* Vol. 45, No. 6, pp. 2867-2875, 1998.

[119] D. L. Chenette, J. D. Tobin and S.P. Geller, "CRRES/SPACERAD Heavy Ion Model of the Environment, CHIME," Hanscom AFB, MA: Phillips Laboratory Report PL-TR-95-2152, 1997.

[120] J. B. Langworthy, "Depletion Region Geometry Analysis Applied to Single Event

Sensitivity," *IEEE Trans. Nuc. Sci.,* Vol. 36, No. 6, pp. 2427-2434, 1989.

[121] P. J. McNulty, W. J. Beauvais, and D.R. Roth, "Determination of SEU Parameters of NMOS and CMOS SRAMs," *IEEE Trans. Nuc. Sci.,* Vol. 38, No. 6, pp. 1463-1470, 1991.

[122] E. L. Petersen, V. Pouget, L. W. Massengill, S. P. Buchner, and D. McMorrow, "Rate Predictions for Single-Event Effects—Critique II," *IEEE Trans. Nuc. Sci.,* Vol. 52, No. 6, pp. 2158-2167, 2005.

[123] E. L. Petersen, "Approaches to Proton Single-Event Rate Calculations," *IEEE Trans. Nuc. Sci.,* Vol. 43, No. 2, pp. 496-504, 1996.

[124] E. L. Petersen, "Interpretation of Heavy Ion Cross Section Measurements," *IEEE Trans. Nuc. Sci.,* Vol. 43, No. 3, pp. 952-959, 1996.

[125] E. L. Petersen, "Single-Event Data Analysis," *IEEE Trans. Nuc. Sci.,* Vol. 54, No. 4, pp. 1392-1405, 2008.

[126] E. L. Petersen, "Parametric and Threshold Studies of Single Event Sensitivity," *IEEE Trans. Nuc. Sci.,* Vol. 55, No. 6, pp. 2319-2841, 2008.

[127] J. C. Pickel, "Single-Event Effects Rate Prediction," *IEEE Trans. Nuc. Sci.,* Vol. 43, No. 2, pp. 483-495, 1996.

[128] R. A. Reed et al., "Heavy Ion and Proton-Induced Single Event Multiple Upset", *IEEE Trans. Nuc. Sci.,* Vol. 44, No. 6, pp. 2224-2229, 1997.

[129] C. S. Guenzer, E. A. Wolicki, and R. G. Allas, "Single Event Upset of Dynamic RAMs by Neutrons and Protons," *IEEE Trans. Nuc. Sci.,* Vol. 26, No. 6, pp. 5048-5052, 1979.

[130] R. C. Wyatt, P. J. McNulty, P. Toumbas, P. L. Rothwell, and R. C. Filz, "Soft Errors Induced by Energetic Protons," *IEEE Trans. Nuc. Sci.,* Vol. 26, No. 6, pp. 4905-4910, 1979.

[131] W.L. Bendel and E.L. Petersen, “Proton Upsets in Orbit”, *IEEE Trans. Nuc. Sci.,* Vol. 30, No. 6, pp. 4481-4485, 1983.

IEEE Transactions on Nuclear Science, Vol. NS-30, No. 6, December 1983

[132] W.J. Stapor, J.P. Meyers2, J.B. Langworthy, and E.L. Petersen, “Two Parameter Bendel Model Calculations for Predicting Proton Inducs Upset,” *IEEE Trans. Nuc. Sci.,* Vol. 37, No. 6, pp. 1966-1973, 1990.

[133] P. Calvel, C. Barillot, P. Lamothe, R. Ecoffet, S. Duzellier, D. Falguere, “An Empirical Model for Predicting Proton Induced Upset,” *IEEE Trans. Nuc. Sci.,* Vol. 43, No. 6, pp. 2827-2832, 1996.

[134] B. Doucin et al., “Characterization of proton interactions in electronic components,” *IEEE Trans. Nuc. Sci.,* Vol. 41, No. 3, pp. 593-600, 1994.

[135] P. J. McNulty, W. G. Abdel-Kader, and J. M. Bisgrove, “Methods for Calculating SEU Rates for Bipoar and NMOS Circuits,” *IEEE Trans. Nuc. Sci.,* Vol. 32, No. 6, pp. 4180-4184, 1985.

[136] Ziegler 1979, J. F. Ziegler and W. A. Lanford, "Effects of Cosmic Rays on Computer memories," *Science,* Vol. 206, pp. 776-788 (1979).

[137] J. R. Letaw and E. Normand, “Guidelines for Predicting Single-Event Upsets in Neutron Environments,” *IEEE Trans. Nuc. Sci.,* Vol. 38, No. 6, pp. 1500-1506, 1991.

[138] E. Normand, “Extensions of the FOM Method – Proton SEL and Atmospheric Neutron SEU,” *IEEE Trans. Nuc. Sci.,* Vol. 51, No. 6, pp. 3494-3504, 1991.

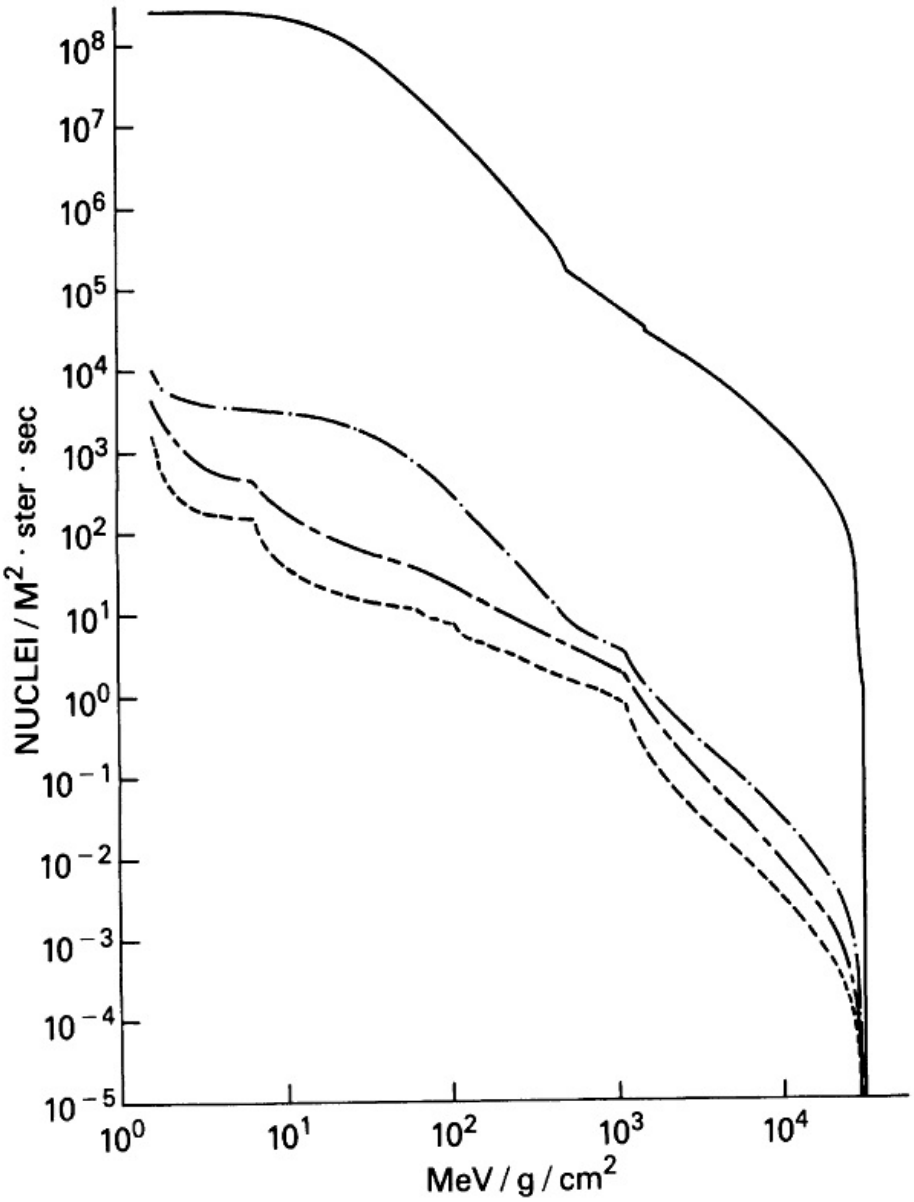

Figure 1: The LET spectra describe the space radiation environment at 1 AU outside the magnetosphere. The spectra are for the peak intensity of the giant solar flare of August 4, 1972 (solid curve); an environment so severe that it will be exceeded only 10 per cent of the time (chain-dot curve); the pure galactic cosmic ray environment at the minimum of the solar activity cycle (chain-dash curve); and the pure galactic cosmic ray environment at the maximum of the solar cycle (dashed curve). This figure is reproduced from figure 1 of [7]. **Permission needed.**

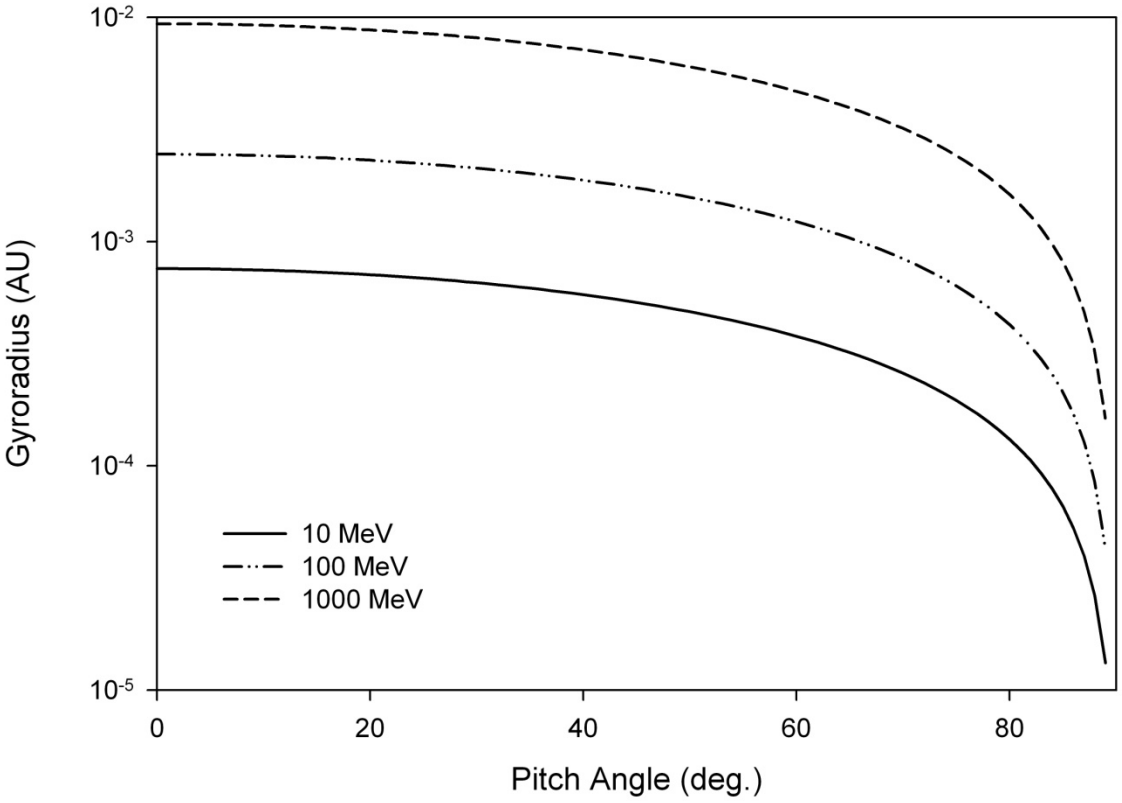

Figure 2: The SEPs follow the interplanetary magnetic field on their way to Earth. Shown here are the gyroradii of 10, 100 and 1000 MeV SPEs at Earth (1 AU) as a function of their pitch angle. This figure shows how closely SEPs are bound to their guiding-center field line.

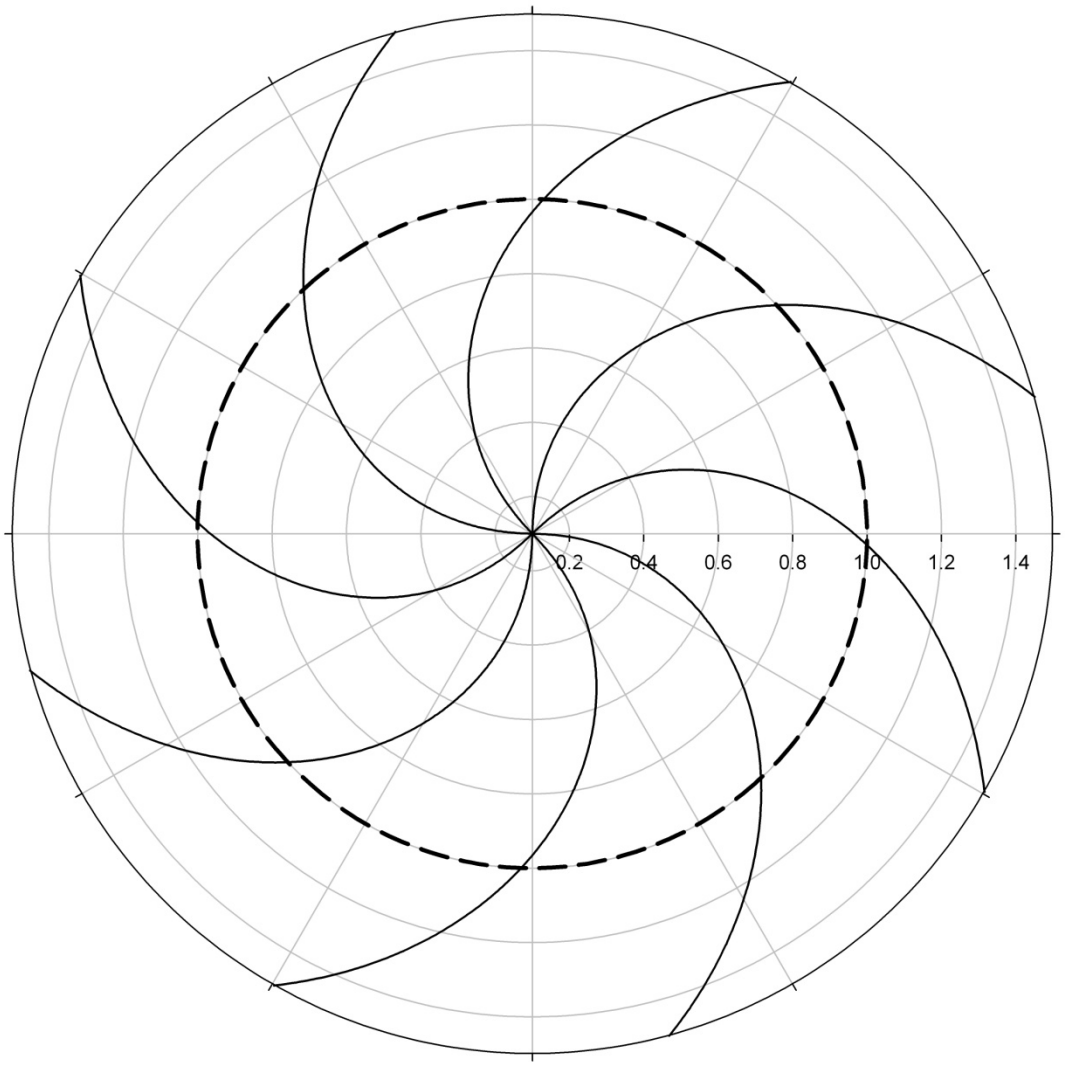

Figure 3: The magnetic field lines are shown in the ecliptic plane as viewed looking down on the north pole of the Sun. The dashed circle is at 1 AU. The eight field lines are shows the Parker Spiral pattern of the interplanetary magnetic field that guides SEPs.

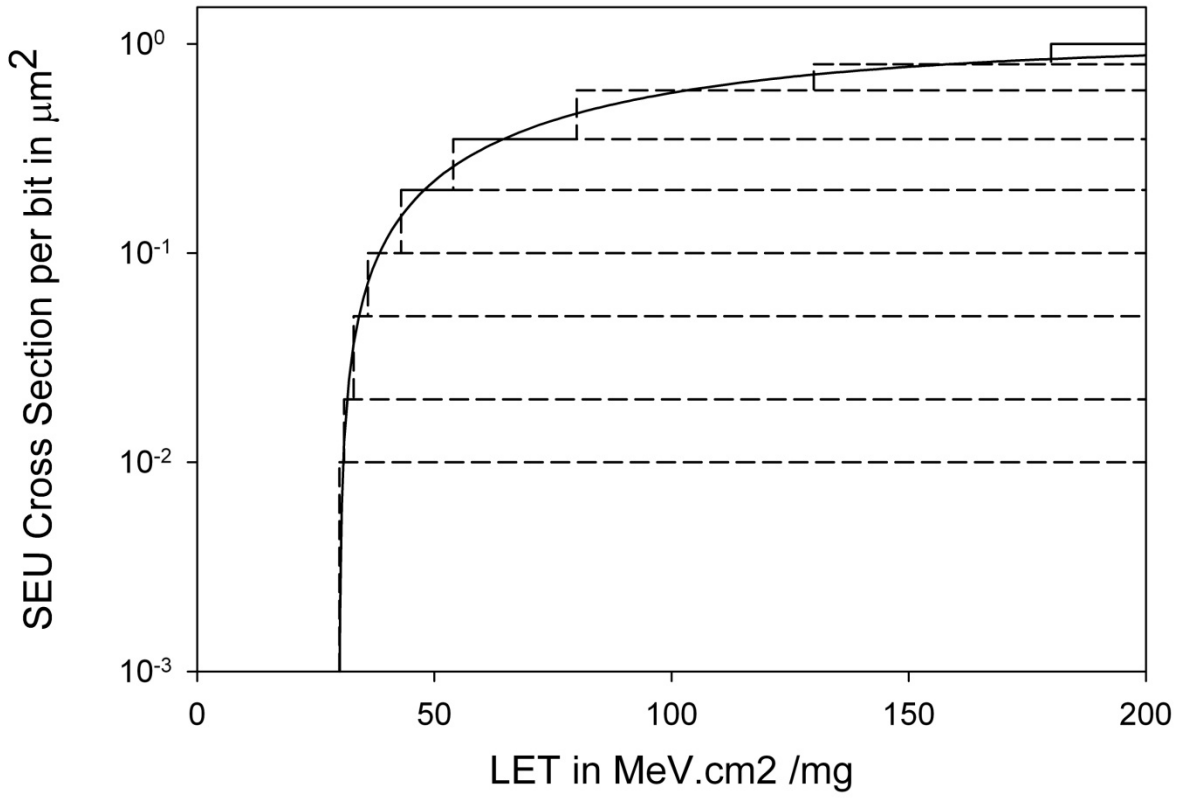

Figure 4: A model of a typical SEU cross section (solid curve) showing how the cross section curve can be represented as a series of steps (dashed lines).